Preferred ground states of a quantum dot under a strong magnetic field

2000 J. Phys.: Condens. Matter 12 3911

(http://iopscience.iop.org/0953-8984/12/16/313)

J. Phys.: Condens. Matter **12** (2000) 3911–3925. Printed in the UK PII: S0953-8984(00)10896-3

Preferred ground states of a quantum dot under a strong magnetic field

W Y Ruan†‡, K S Chan‡, H P Ho‡ and E Y B Pun§

† Department of Applied Physics, South China University of Technology, Guangzhou 510641, People's Republic of China
‡ Department of Physics and Materials Science, City University of Hong Kong, Hong Kong, People's Republic of China
§ Department of Electronic Engineering, City University of Hong Kong, Hong Kong, People's Republic of China

E-mail: phwyruan@scut.edu.cn (W Y Ruan)

Received 2 January 2000, in final form 14 March 2000

Abstract. The ground-state energies of several interacting electrons confined in a parabolic dot in two dimensions are obtained by using hyperspherical coordinates and high-order perturbation theory. The effect of a perpendicular magnetic field is to change the ground state discontinuously in orbital angular momentum L. The preferred values of L for the ground state and the associated electronic structures are studied in detail. It is found that the effective interaction between two electrons moving in different cyclic orbits is a short-range attraction matched to a long-range repulsive tail. Because of this, electrons tend to fill adjacent cyclic orbits and form bunches in the ground states. The effects of an impurity ion are also considered.

1. Introduction

The electronic structure in quantum-dot systems is now a topic under intensive study [1]. Recent experiments on single-electron tunnelling into a quantum dot [2, 3] have demonstrated the possibility of measuring the chemical potential μ_N of an N-electron system. μ_N is defined as the energy required to add one electron to the dot:

$$\mu_N = E(N) - E(N-1) \tag{1}$$

where $E(N)$ is the ground-state energy of an N-electron dot, etc. Hence, the measurement of μ_N allows one to determine the ground-state energies indirectly. In a varying magnetic field, the experimentally measured μ_N show many kinks [1], stimulating many theoretical calculations of the μ–B phase diagrams [4, 5]. In the weak-field regime, the kinks can be fully understood by considering an independent-particle model: they are caused by the jump of the highest-energy electron in the dot from one discrete quantum level into another. In the strong-field regime, where all electrons are in the lowest Landau level and spin polarized, the kinks signal collective transitions induced by the electron–electron interaction and cannot be explained within the single-electron picture. In this case, the central issue to be addressed is that of what kinds of electronic structure stabilize the ground state of N interacting electrons.

In circular dots where the total angular momentum is a good quantum number, the electron correlations result in extra stable ground states with magic values of the angular momentum

0953-8984/00/163911+15$30.00

L. For dots with a small number of electrons ($N \leqslant 7$), two sequences of magic angular momenta, i.e.,

$$L_a = Nk + N(N-1)/2 \qquad (k = 0, 1, 2, \ldots) \tag{2}$$

and

$$L_b = (N-1)(k+1) + (N-1)(N-2)/2 \qquad (k = 1, 2, 3, \ldots) \tag{3}$$

have been found [6–15]. The ground-state transitions induced by a varying magnetic field strictly obey the rules $\Delta L = N$ for $N \leqslant 5$, and $\Delta L = N - 1$ for $N = 6, 7$ in the spin-polarized regime. States with other non-magic L-values can never become the ground state. For these rules, the geometric configuration model [12] provides a simple and reasonable explanation. According to the model, there is a large probability for few interacting electrons to form a regular polygon in the ground state, i.e., an N-sided regular polygon with one particle at each vertex when $N \leqslant 5$ or an $(N-1)$-sided polygon with the Nth particle at the centre when $N = 6$ and 7, in order to minimize the pairwise Coulomb repulsion. Unfortunately, such energetically favourable configurations are generally prohibited by the basic laws of quantum mechanics. From a consideration of the exchange and rotational symmetries [12], the N-sided polygon is allowed only when

$$L = Nk + N(N-1)/2$$

and the $(N-1)$-sided polygon is allowed only when

$$L = (N-1)(k+1) + (N-1)(N-2)/2.$$

These are just the magic numbers given by equations (2) and (3). Other models, such as the composite-fermion model [16, 17] and Dharma-wardana's model [18], also explain the existence of magic numbers with partial success.

Despite the success of the geometric configuration model in explaining the magic L-values of few-electron systems, there are still sufficient reasons to question its applicability to several-electron systems. First of all, it is known that the lowest-energy configuration of a classical several-electron system is a multi-shell structure [15, 16] which does not have any rotational symmetry as a regular polygon, unless, as on some rare occasions, the numbers of particles in different shells happen to be commensurable. Therefore, for the majority of cases, there should be no restriction on the occupation of the lowest-energy configuration arising from exchange and rotational symmetries. But the fact remains that magic numbers exist in systems with any number of particles (see below). Secondly, a several-electron system may have a few equilibrium configurations which are very close in energies. Therefore, the system has multiple choices of electronic structures for minimizing the ground-state energy, a feature not shared by systems with few electrons. Finally, unlike those of few-particle systems, the wavefunctions of a several-particle system are generally very smooth. The assumption of forming certain regular polygons does not have a firm grounding.

This paper reports our analysis as regards the magic L-values of a quantum dot with $N = 9$, 10, and 11, and the associated electronic structures, which, as far as we know, have not been studied by exact diagonalizations and including the mixings of several Landau levels, due to the enormous number of basis functions involved. By introducing hyperspherical coordinates, we have succeeded in separating the Schrödinger equation into a B-independent hyper-angular equation and a B-dependent hyper-radial equation. The latter is solved by employing the high-order perturbation theory to obtain the ground-state energies. We find that the orbiting electrons in a quantum dot tend to form bunches. A more general formula is derived for determining the magic numbers, of which equations (2) and (3) are two special cases. The *bunching* behaviour can be understood in terms of a short-range attraction between two orbiting electrons in the lowest Landau level.

2. The model

Consider a droplet of spinless (spin-polarized) 2D electrons confined in a parabolic potential, $m_e^*\omega_0^2 r^2/2$, where ω_0 is a strength parameter, and m_e^* is the effective mass. A magnetic field B is applied in the vertical direction. The N-body Schrödinger equation in the symmetric gauge reads [9]

$$\left\{\sum_{j=1}^{N}\left[\frac{p_j^2}{2m_e^*}+\frac{1}{2}m_e^*\omega^2 r_j^2\right]-\frac{\omega_c\hbar}{2}L+\frac{e^2}{4\pi\epsilon_0\epsilon_r}\sum_{j>k}^{N}\frac{1}{r_{jk}}\right\}\Psi=E\Psi \tag{4}$$

where

$$\omega=\sqrt{\omega_0^2+\omega_c^2/4}$$

and $\omega_c = eB/m_e^*$ is the cyclotron frequency.

When the length unit is the effective cyclotron radius $a = (\hbar/2\omega m_e^*)^{1/2}$ and the energy unit is $\hbar\omega$, equation (4) can be rewritten as

$$\left\{\sum_{j=1}^{N}\left[-\nabla_j^2+\frac{1}{4}r_j^2\right]+\gamma\sum_{j>k}^{N}\frac{1}{r_{jk}}\right\}\Psi=(E+\zeta L)\,\Psi \tag{5}$$

where $\gamma = 2a/a_B$, $a_B = 4\pi\epsilon\hbar^2/(e^2m_e^*)$ is the effective Bohr radius, $\zeta = \omega_c/(2\omega)$.

We use z_j ($\equiv x_j + \mathrm{i}y_j$) to denote the complex position of the jth electron and introduce a set of hyperspherical coordinates in the following manner [19]:

$$z_j=\rho\left(\prod_{k=0}^{j-1}\sin\phi_k\right)\cos\phi_j\exp(\mathrm{i}\varphi_j)\qquad(j=1,2,\ldots,N) \tag{6}$$

where φ_j is the polar angle of z_j,

$$\rho=(|z_1|^2+|z_2|^2+\cdots+|z_N|^2)^1/2$$

is the hyper-radius, $\{\phi_1,\phi_2,\ldots,\phi_{N-1}\}$ are the hyper-angles, defined in the domain $0\leqslant\phi_j\leqslant\pi/2$, and $\phi_0\equiv\pi/2$ and $\phi_N\equiv 0$ are understood. With hyperspherical coordinates, equation (5) takes the form

$$\left[-\frac{1}{\rho^{2N-1}}\frac{\partial}{\partial\rho}\rho^{2N-1}\frac{\partial}{\partial\rho}+\frac{\Lambda^2(\Omega)}{\rho^2}+\frac{1}{4}\rho^2+\gamma\frac{U(\Omega)}{\rho}\right]\Psi(\rho,\Omega)=(E+\zeta L)\Psi(\rho,\Omega) \tag{7}$$

where Ω represents all angular variables,

$$U(\Omega)=\rho\sum_{i<j}^{N}1/r_{ij}$$

and $\Lambda^2(\Omega)$ is the grand orbital operator. The eigenfunctions of the eigenequation

$$\Lambda^2(\Omega)Y_{[\lambda]}(\Omega)=\lambda(\lambda+2N-2)Y_{[\lambda]}(\Omega)$$

are known as hyperspherical harmonics which can be expressed as

$$Y_{[\lambda]}(\Omega)=\left[\prod_{j=1}^{N-1}P_{j,\nu_j}^{\lambda_{j+1},|l_j|}(\phi_j)\right]\left[\prod_{k=1}^{N}\frac{\exp(\mathrm{i}l_k\varphi_k)}{\sqrt{2\pi}}\right] \tag{8}$$

where $[\lambda]$ represents a set of $(2N-1)$ quantum numbers $\nu_1,\ldots,\nu_{N-1},l_1,\ldots,l_N,\lambda_N=|l_N|$, $\lambda_j=2\nu_j+\lambda_{j+1}+|l_j|$,

$$\lambda=\sum_{j=1}^{N-1}(2\nu_j+|l_j|)+|l_N|\qquad L=\sum_{k=1}^{N}l_k$$

and

$$P_{j,\nu}^{\alpha,\beta}(\phi) = \left[\frac{2(2\nu+\alpha+\beta+1)\nu!(\nu+\alpha+\beta)!}{(\nu+\alpha)!(\nu+\beta)!}\right]^{1/2} \sum_{m=0}^{\nu}(-1)^{\nu-m}\binom{\nu+\alpha+N-j-1}{m} \times \binom{\nu+\beta}{\nu-m}(\cos\phi)^{2m+\beta}(\sin\phi)^{2(\nu-m)+\alpha}. \tag{9}$$

By expanding $\Psi(\rho, \Omega)$ in terms of the antisymmetrized hyperspherical harmonics $\tilde{Y}_{[\lambda]}(\Omega)$:

$$\Psi(\rho, \Omega) = \sum_{[\lambda]} F_{[\lambda]}(\rho)\tilde{Y}_{[\lambda]}(\Omega) \tag{10}$$

equation (7) is transformed into a set of coupled differential equations:

$$\left[\frac{1}{\rho^{2N-1}}\frac{\mathrm{d}}{\mathrm{d}\rho}\rho^{2N-1}\frac{\mathrm{d}}{\mathrm{d}\rho} - \frac{\lambda(\lambda+2N-2)}{\rho^2} - \frac{1}{4}\rho^2 + E + \zeta L\right] F_{[\lambda]}(\rho) = \gamma\sum_{[\lambda']}\frac{U_{[\lambda],[\lambda']}}{\rho}F_{[\lambda']}(\rho) \tag{11}$$

where

$$U_{[\lambda],[\lambda']} = \int \tilde{Y}^*_{[\lambda]}(\Omega)U(\Omega)\tilde{Y}_{[\lambda']}(\Omega)\,\mathrm{d}\Omega \tag{12}$$

are the coupling constants.

Equations (11) remain exact. If $\gamma = 0$, they can be solved analytically and completely:

$$F^{(0)}_{n,\lambda}(\rho) = \left(\frac{n!}{2^\alpha(n+\alpha)!}\right)^{1/2}\rho^\lambda L_n^{(\alpha)}(\rho^2/2)\exp(-\rho^2/4) \tag{13}$$

$$E^{(0)}_n = 2\left(n + \frac{\lambda - L}{2}\right) + N + (1-\zeta)L \qquad (n = 0, 1, 2, \ldots) \tag{14}$$

where $\alpha = \lambda + N - 1$. Here, $[n + (\lambda - L)/2]$ gives the Landau-level index. $L_n^{(\alpha)}(x)$ is a Laguerre polynomial.

When $\gamma \neq 0$, the approximation that we use this paper is truncating the expansion series for $\Psi_{[\lambda]}(\rho, \Omega)$ in equation (10) such that the summation only runs over the hyperspherical harmonics associated with the smallest λ (note that $\lambda_{min} = L$). When $\lambda = L$, i.e., $\nu_j = 0$ for all j, the antisymmetrized hyperspherical harmonics $\tilde{Y}_{[\lambda]}(\Omega)$ can be expressed as a Slater determinant:

$$|l_1 \cdots l_N; L\rangle = \left[\prod_{j=1}^{N} 2\pi(2l_j)!!\right]^{-1/2} \mathrm{Det}\left\{\hat{z}_1^{l_1}, \hat{z}_2^{l_2}, \ldots, \hat{z}_N^{l_N}\right\} \tag{15}$$

where $\hat{z}_j = z_j/\rho$.

When we write $F_{[\lambda]}(\rho)$ as

$$F_{[\lambda]}(\rho) = G_L(\rho)u_{l_1\cdots l_N} \tag{16}$$

equations (11) can be reduced to a second-order differential equation:

$$\left[\frac{\mathrm{d}^2}{\mathrm{d}\rho^2} + \frac{2N-1}{\rho}\frac{\mathrm{d}}{\mathrm{d}\rho} - \frac{L(L+2N-2)}{\rho^2} - \frac{1}{4}\rho^2 - \frac{\tilde{\eta}}{\rho} + E + \zeta L\right] G_L(\rho) = 0 \tag{17}$$

and a matrix eigenequation:

$$\bar{\mathbf{U}}\bar{u} = \eta\bar{u} \tag{18}$$

where $\bar{\mathbf{U}}$ is a square matrix composed of $U_{l_1\cdots l_N;l'_1\cdots l'_N}$, $\bar{u}$ is the column matrix of $u_{l_1\cdots l_N}$, η is the eigenvalue obtained by numerically diagonalizing $\bar{\mathbf{U}}$, $\tilde{\eta} = \gamma\eta$.

To obtain the eigenenergies from equation (17), we treat as a perturbation the Coulomb term $H' = \beta\tilde{\eta}/\rho$, where β is a strength parameter set to unity at the end. The energy eigenvalue and eigenfunction of the nth state are expressed as power series in β:

$$E_n = \sum_{j=0}^{\infty} \beta^j E_n^{(j)} \tag{19}$$

$$G_{n,L}(\rho) = \sum_{j=0}^{\infty} \beta^j G_{n,L}^{(j)}(\rho). \tag{20}$$

Substituting equations (19) and (20) into equation (17) and setting the coefficient of each β^j to zero, we obtain the following recurrence relations for determining $E_n^{(j)}$:

$$E_n^{(1)} = H'_{nn} \tag{21}$$

$$D_{kn}^{(1)} = \begin{cases} \dfrac{H'_{kn}}{E_n^{(0)} - E_k^{(0)}} & \text{for } k \neq n \\ 0 & \text{for } k = n \end{cases} \tag{22}$$

and for $j \geqslant 2$:

$$E_n^{(j)} = \sum_k H'_{nk} D_{kn}^{(j-1)} \tag{23}$$

$$D_{kn}^{(j)} = \begin{cases} \dfrac{1}{E_n^{(0)} - E_k^{(0)}} \left[\displaystyle\sum_{k'} H'_{kk'} D_{k'n}^{(j-1)} - \sum_{j'=1}^{j-1} E_n^{(j')} D_{kn}^{(j-j')} \right] & \text{for } k \neq n \\ 0 & \text{for } k = n \end{cases} \tag{24}$$

where

$$\begin{aligned} H'_{nk} &= \int_0^{\infty} F_{n,L}^{(0)}(\rho) H' F_{k,L}^{(0)}(\rho) \rho^{2N-1} \, \mathrm{d}\rho \\ &= \tilde{\eta} \left[\frac{\pi n! k!}{2^{2\alpha+1}(n+\alpha)!(k+\alpha)!} \right]^{1/2} \\ &\quad \times \sum_{m=0}^{n} \sum_{m'=0}^{k} (-1)^{m+m'} \binom{n+\alpha}{n-m} \binom{k+\alpha}{k-m'} \frac{[2(m+m'+\alpha)-1]!!}{2^{m+m'} m! m'!}. \end{aligned} \tag{25}$$

It is interesting to notice that the usual approach, i.e. assuming that all particles occupy the lowest Landau level [16], is equivalent to the first-order perturbation theory in our present formalism. From equations (18), (19), (21), and (25), we obtain the explicit expression for the ground-state energy in the first-order perturbation theory:

$$E_0 \approx E_0^{(0)} + E_0^{(1)} = N + (1-\zeta)L + \tilde{\eta} \frac{(2\alpha-1)!!}{(2\alpha)!!} \left(\frac{\pi}{2} \right)^{1/2}. \tag{26}$$

Finally [20], we would like to point out the existence of exact solutions of equation (17) at some special values of $\tilde{\eta}$ (note that $\tilde{\eta}$ depends on the adjustable parameter B through γ). To find these solutions, we write G_λ as a product of asymptotic solutions (near $\rho = 0$ and ∞) and a power series in ρ:

$$G_\lambda(\rho) = \rho^\lambda \exp(-\rho^2/4) \sum_\nu C_\nu \rho^\nu. \tag{27}$$

Substitution of equation (27) into equation (17) leaves us with a set of linear equations for determining the expansion coefficients $\{C_\nu\}$:

$$(2\alpha + 1)C_1 - \tilde{\eta}C_0 = 0 \tag{28}$$

and

$$\nu(2\alpha + \nu)C_\nu - \tilde{\eta}C_{\nu-1} + [\epsilon - \nu + 2]\, C_{\nu-2} = 0 \tag{29}$$

where $\epsilon = E - N - (1 - \zeta)L = E - E_0^{(0)}$.

The three-step nature of the recurrence relation of equation (29) implies that if two succeeding coefficients (say $C_{\nu+1}$ and $C_{\nu+2}$) vanish, the other $C_{\nu'}(\nu' > \nu + 2)$ vanish automatically. Since equations (28) and (29) allow C_ν to be expressed in terms of C_0 in the following manner:

$$C_\nu = H(\nu, \epsilon, \tilde{\eta})C_0 \tag{30}$$

adherence to the conditions $C_{\nu+2} = 0$ and $C_{\nu+1} = 0$ is guaranteed if

$$H(\nu + 1, \epsilon, \tilde{\eta}) = 0 \tag{31}$$

and

$$\epsilon = \nu. \tag{32}$$

Both equations determine the spectrum of the allowed $\tilde{\eta}$ and E. This is very useful for checking the accuracy of the perturbation theory.

3. Numerical results and interpretations

3.1. Convergence of the perturbative expansion

To study the convergence of the perturbative expansion of equation (19), we first find the zeros of equation (31). For a given ϵ, there are several $\tilde{\eta}$-solutions. The largest solution gives the ground state since the corresponding wavefunction has no node. Presented in the first row of table 1 are the largest $\tilde{\eta}$-solutions associated with $\epsilon = 10$, 20, 30, and 40 respectively. With these $\tilde{\eta}$-values as the input, the ground-state energies are recalculated from equations (19)–(25). In table 1, results with the first five orders of perturbation are presented for nine electrons in the $L = 36$ state and compared with the exact ones, where the convergence is fast when $\tilde{\eta}$ is small but slows down as $\tilde{\eta}$ increases. For a typical dot in GaAs (i.e., $m_e^* = 0.067m_e$, $\epsilon_r = 13.1$, and $\hbar\omega_0 = 3.6$ meV) under a magnetic field $B = 5$ T, we obtain $\tilde{\eta} = 376.5$ for the $L = 36$ state. Hence the error in the perturbative expansion is no more than a fraction in

Table 1. The calculated lowest-energy eigenvalues (ϵ) of the state with $L = 36$ for a system with $N = 9$ at four different $\tilde{\eta}$-values where analytical solutions of equation (17) exist. j_m is the highest order of perturbation included.

	$\tilde{\eta}$			
j_m	96.720258942	198.71195983	305.92050170	418.26510470
1	10.281165492	21.122674471	32.518722964	44.460724239
2	9.9838458368	19.867694677	29.544278357	38.900504095
3	10.000932826	20.015873184	30.084956660	40.282376977
4	9.9999593951	19.998529899	29.987531824	39.941935955
5	10.000000021	20.000017000	30.000392487	40.003379831
Exact	10	20	30	40

10^3 when the first five orders are included. For larger L-values and B, $\tilde{\eta}$ is smaller and the expansion in equation (19) converges even faster. Another noteworthy point in table 1 is that the ground-state energies oscillate with the order of perturbation. As a result, the extensively used second-order perturbation theory [21] significantly underestimates the ground-state energies.

3.2. The preferred ground states

In figure 1, the lowest eigenenergies associated with different L-values, obtained from equation (19), are presented as a function of field strength B for $N = 9$, 10, and 11. There are complicated level-crossings as the external magnetic field is varied. Changes in the L-values of the ground state of the system can be simply understood from equation (26), where only the first order of perturbation is considered: in the weak-field regime, where ζ is close to zero and $E_0^{(0)}$ is dominant, the ground-state energy can be minimized by minimizing L. Then electrons tend to fill the innermost orbits with single-particle angular momenta $l = 0, 1, 2, \ldots, (N-1)$, and the system has a ground state with $L = N(N-1)/2$, the smallest total angular momentum allowed by the Pauli principle in the lowest Landau level. As the magnetic field increases, $E_0^{(0)}$ decreases and the Coulomb energy tends to grow due to the reduction of the effective magnetic length a. The ground-state energy can be minimized by an increase in L since the Coulomb energy decreases with increasing L (see below). Consequently the dot undergoes a series of transitions to ground states with higher and higher angular momenta L to lower the ground-state energy. Each of these transitions causes a kink in the gate voltage applied to the dot in experiments [1]. The transitions are discontinuous, i.e., $L = 36 \to 45 \to 52 \to 57 \to 64 \to 71 \to \cdots$ for $N = 9$, $L = 45 \to 55 \to 61 \to 63 \to 69 \to 77 \to \cdots$ for $N = 10$ and $L = 55 \to 66 \to 73 \to 79 \to 82 \to 87 \to \cdots$ for $N = 11$. These are the magic values of L. Obviously, equations (2) and (3) are inadequate to describe all of these magic numbers, indicating that the complexity increases with increasing N. States with other L-values exist at much higher energy levels and can never become the ground state no matter what values of B and ω_0 are taken.

In order to trace the origin of the magic numbers, η_0, the lowest eigenvalue of matrix $\bar{\mathbf{U}}$ is plotted as a function of L in figure 2, where η_0 shows rich structures although it tends to decrease globally. Each state where the ground state can occur gives a deep downward cusp in η_0. Generally speaking, the deeper the cusp, the wider the range of B-field over which the corresponding state is the ground state. The depths of, and the separations from the adjacent downward cusps also affect this range. In figure 2, there are also some states which give a downward cusp but fail to become the ground state (e.g., $L = 50, 54, 60, 66, \ldots$ for $N = 9$). As an example, consider the state with $L = 73$ for $N = 10$. This state clearly shows a significant downward cusp but fails to form a ground state (see figure 1). The reason is that the cusps produced by the $L = 69$ and $L = 77$ states are too deep.

3.3. Classification of the states

At first sight, the downward cusps in figure 2 appear quite irregular. Analysis of the structures of the corresponding angular wavefunctions reveals that although they are linear combinations of many basis states of $|l_1, l_2, \ldots, l_N; L\rangle$, only one of the basis states is dominant. For example, for $N = 9$ in the state with $L = 71$, the $u_{l_1 \cdots l_N}$ associated with the basis state $|0, 1, 7, 8, 9, 10, 11, 12, 13; 71\rangle$ is significantly larger than other $u_{l_1 \cdots l_N}$, while for $N = 9$ and $L = 68$, the eigenstate is dominated by the basis state $|0, 5, 6, 7, 8, 9, 10, 11, 12; 68\rangle$, and so on. This can also be seen clearly from the distribution of the occupation numbers w_l (see

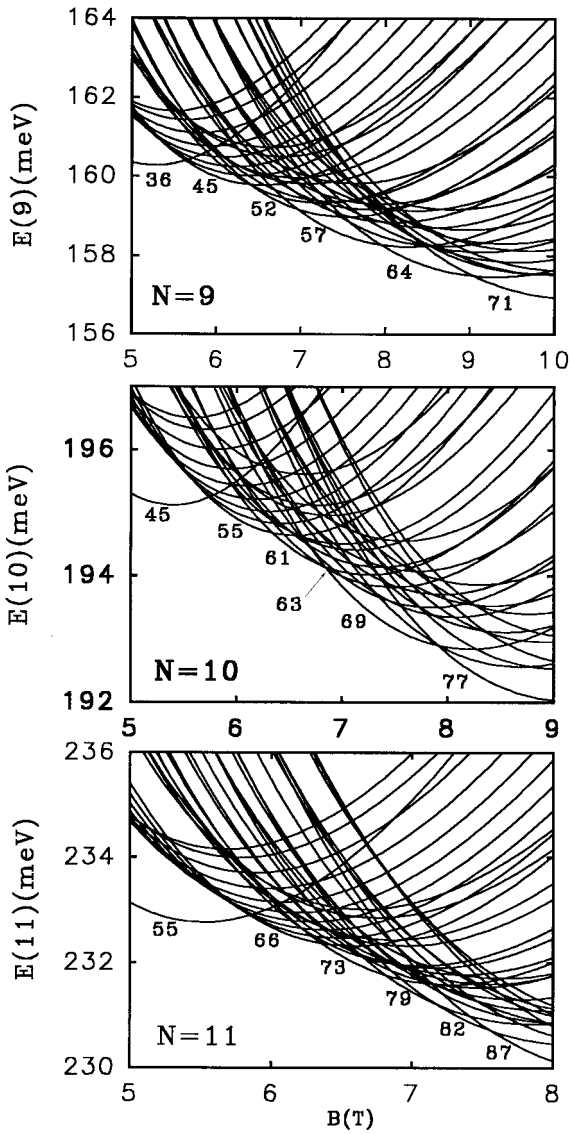

Figure 1. The lowest eigenenergies associated with different L-values, given by equation (19), are presented as a function of field strength B for $N = 9$, 10, and 11. The zero-point energy $N\hbar\omega$ is omitted. Numbers in the figures label the ground-state angular momentum L. The values $\hbar\omega_0 = 3.6$ meV, $m_e^* = 0.067m_e$, $\epsilon_r = 13.1$ have been used.

figures 3–5), which is defined by

$$w_l = \sum_{l_1 \cdots l_N} |u_{l_1 \cdots l_N}|^2 \langle l_1, \ldots, l_N; L|\hat{a}_l^\dagger \hat{a}_l|l_1, \ldots, l_N; L\rangle \tag{33}$$

where $\hat{a}_l^\dagger(\hat{a}_l)$ is an operator that creates (destroys) an electron with angular momentum l. w_l is the probability of finding an electron in the lth orbit and is related to the total angular

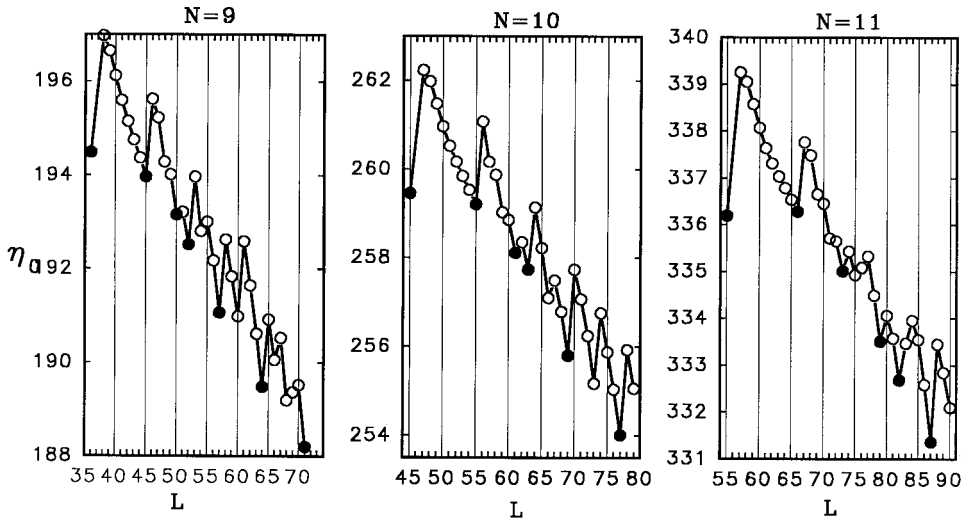

Figure 2. The lowest eigenvalues of the matrix $\bar{\mathbf{U}}$ are presented as a function of L for $N = 9$, 10, and 11. The black dots denote states which can become the ground state in a varying magnetic field.

momentum L by

$$L = \sum_l l w_l. \tag{34}$$

The states presented in figures 3–5 show clearly bunch structures in their w_l-distribution. As a general rule, given N electrons, n of them occupying the innermost orbits $l = 0, 1, \ldots, n-1$, and the other $(N-n)$ occupying the outer orbits $l = n+k, n+k+1, \ldots, n+k+N-n-1$ $(k \geqslant 1)$ compactly, the basis state will have a total angular momentum

$$L = (N-n)(k+n) + [(n-1)n + (N-n-1)(N-n)]/2 \qquad (k = 1, 2, \ldots). \tag{35}$$

In figures 3–5, states in the same column have similar bunch structures since they are dominated by basis states having the same n and $N-n$, but differing in k. Hence we can use the symbol $|\{n, N-n\}_k; L\rangle$ to denote an eigenstate and characterize the dominant electronic structure of states with a magic L-value: n is the number of electrons in the inner bunch, $(N-n)$ is the number of electrons in the outer bunch, k is the number of holes between the two bunches, L is related to n, $(N-n)$, and k through equation (35). States with non-magic L-values do not have a clear bunch structure and the symbol is inadequate. It is interesting to note that equations (2) and (3) can be regarded as two special cases of equation (35) with $n = 0$ and 1 respectively.

For $N = 9$, 10, and 11, only two magic eigenstates of $|\{0, N\}_k; L\rangle$ with $k = 0$ and 1 have been found (see the left-hand columns of figures 3, 4, and 5). They are the two smallest magic L-values in the systems. With a small L (i.e., $L \leqslant N + N(N-1)/2$), where only very limited single-particle orbits are open to the system, the splitting of the full N-electron bunch into two smaller bunches of $\{n, N-n\}$ with $n < (N-n)$ is either impossible or the resulting two bunches are so close together that there is only one hole between them (e.g., see figure 3 for $N = 9$ and $L = 42$). The systems preferred a ground state with all of the electrons being kept in a compact bunch. As L increases, magic L-values associated with other bunch structures are available.

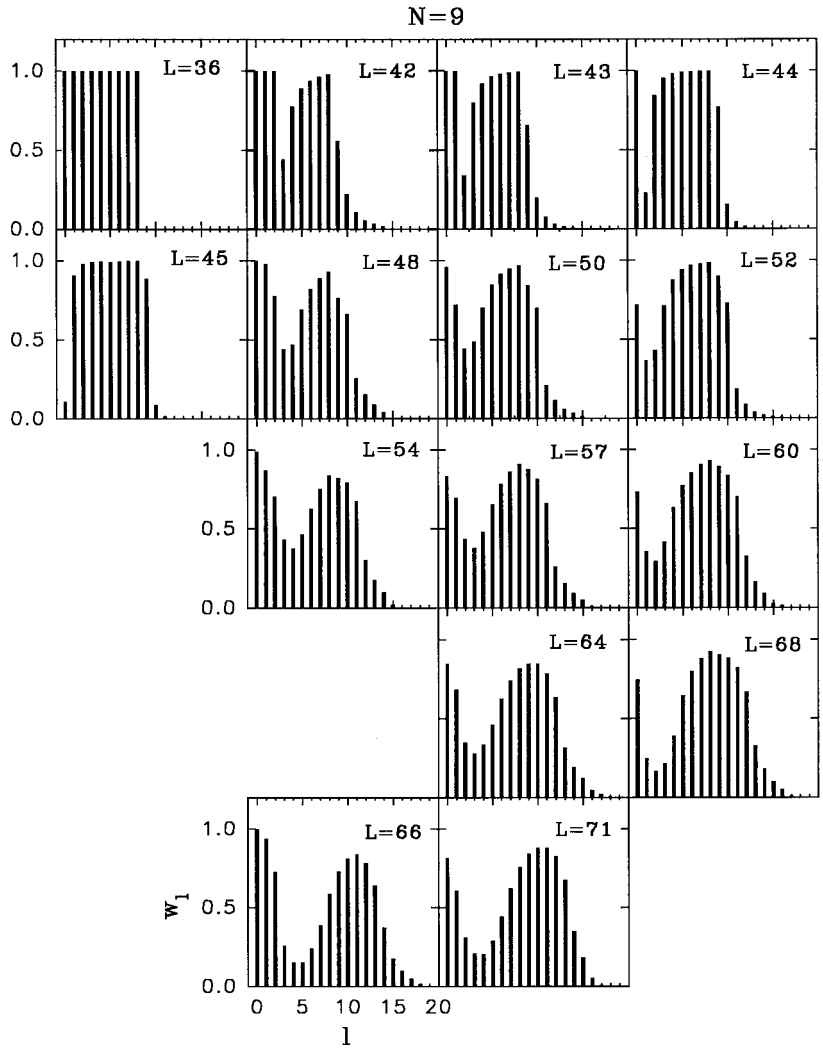

Figure 3. The distribution of occupation numbers w_l for $N = 9$ and states which show a clear bunch structure.

For $N = 9$, the most strongly preferred sequence of states as regards the ground state occurring are $|\{2, 7\}_k; L\rangle$, when L is sufficiently large. This can be seen from figure 1, where states $|\{2, 7\}_3; 57\rangle$, $|\{2, 7\}_4; 64\rangle$, $|\{2, 7\}_5, 71\rangle$, ... have a wider B-range over which they can become the ground state. This implies that the bunch structure of $\{2, 7\}$ is most effective in reducing the Coulomb energy. In figure 3, the state with $L = 60$ is a very special case, i.e., the basis states $|0, 1, 2, 7, 8, 9, 10, 11, 12; 60\rangle$ and $|0, 4, 5, 6, 7, 8, 9, 10, 11; 60\rangle$ are both involved. If the former is dominant, the eigenstate should be denoted as $|\{3, 6\}_4; 60\rangle$; if the latter is dominant, the eigenstate should be denoted as $|\{1, 8\}_3; 60\rangle$, according to the regulation introduced above. In practice, the basis state $|0, 4, 5, 6, 7, 8, 9, 10, 11; 60\rangle$ is found to be dominant. This is why the state is given in the right-hand column and there is a gap between states $L = 54$ and $L = 66$ in the second column (from the left) in figure 3.

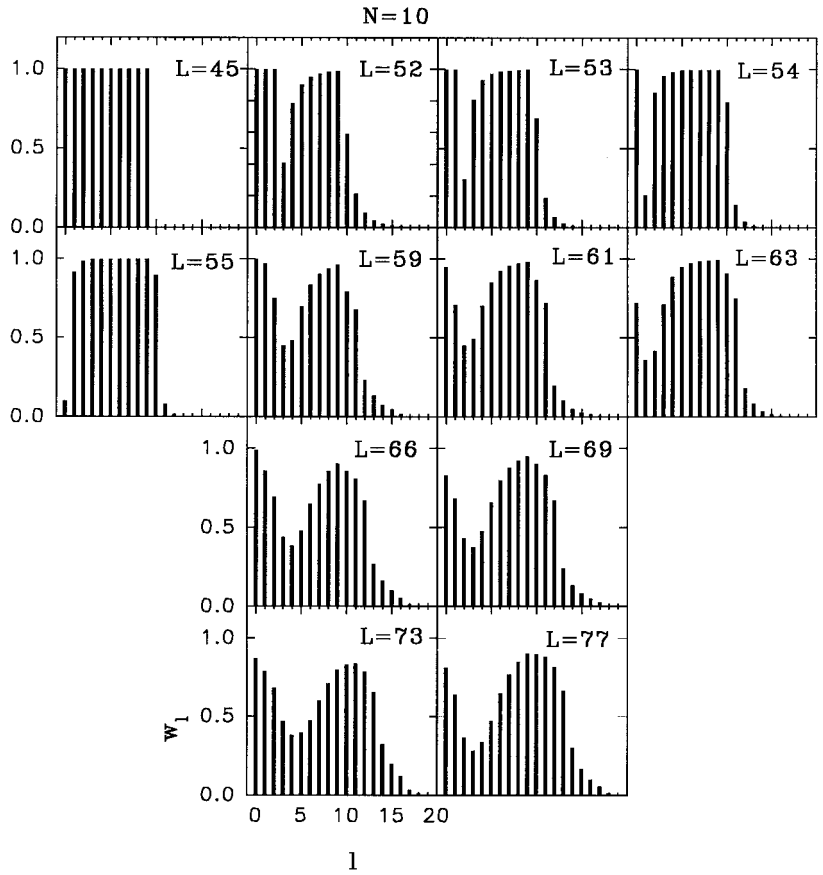

Figure 4. As figure 3, but for $N = 10$.

For $N = 10$, the most strongly preferred sequence of states is $|\{2, 8\}_k; L\rangle$ since the states $|\{2, 8\}_2; 61\rangle$, $|\{2, 8\}_3; 69\rangle$, $|\{2, 8\}_4; 77\rangle$, ... have a wider B-range over which they can become the ground state in figure 1. Hence, the most stable bunch structure is $\{2, 8\}$ for $N = 10$.

For $N = 11$, for the states $|\{2, 9\}_2; 73\rangle$, $|\{2, 9\}_3; 82\rangle$, ... and the states $|\{3, 8\}_3; 79\rangle$, $|\{3, 8\}_4; 87\rangle$, ..., the B-ranges over which they can become the ground state are about the same. This implies that the bunch structures $\{2, 9\}$ and $\{3, 8\}$ are almost equally effective for $N = 11$ in reducing the Coulomb energy.

3.4. Theoretical interpretations

To answer the question of why the formation of bunches can effectively reduce the Coulomb energy, in figure 6, $\langle l_1, l_2|v(1, 2)|l_1, l_2\rangle$, the Coulomb interaction energy of two electrons in an unperturbed state $|l_1, l_2\rangle$, is presented as a function of $\Delta \equiv |l_2 - l_1|$ for different values of $L_{12} \equiv l_1 + l_2$. Figure 6 reveals that for a given L_{12}, there are essentially two extreme options in reducing the interaction energy: $\Delta = 1$ or $\Delta = L_{12}$. With $\Delta = 1$ (note that $\Delta = 0$ is prohibited by the Pauli principle), the two electrons move around with the closest angular momenta and meet each other least frequently, resulting in a state with low interaction energy. In the classical limit (i.e., $l_1, l_2 \gg 0$), this would be a state of two electrons moving at about

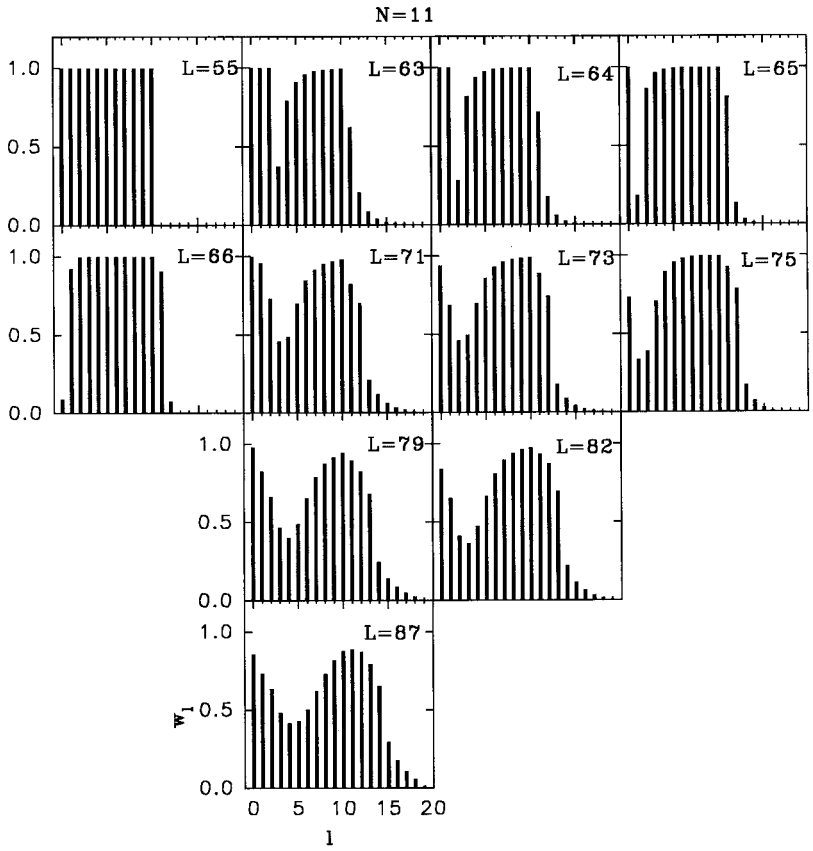

Figure 5. As figure 3, but for $N = 11$.

the same speed and with a phase difference of π (resulting from antisymmetrization). With $\Delta = L_{12}$, the two electrons move in orbits that are as far apart as possible.

An alternative and more comprehensive view of this subject is to regard the cyclic motion of an electron as a *quasiparticle* and Δ as a parameter denoting the separation of two quasiparticles. Then figure 6 just tells us that the mutual interaction between two quasiparticles is a short-range attraction matched to a long-range repulsive tail (Hartree–Fock calculations also suggested the existence of a short-range attraction; see [22]). Hence electrons tend to fill the adjacent orbits to minimize their interaction energy. The short-range attraction will be saturated when the number of electrons in a bunch is up to a certain maximum. The interaction between two saturated bunches is repulsive and they tend to separate from one another. Figure 6 also indicates that the range of attraction is shorter in the inner orbits (i.e., when L_{12} is small and thus both l_1 and l_2 are small). Hence the inner bunch is always composed of a smaller number of particles than the outer bunch.

It is well known that in the large-L limit, the Coulomb energy overwhelms the kinetic energy and the system tends to crystallize. In the range of L covered above, the distribution of the wavefunctions in multi-coordinate space is still rather smooth and the geometric structures are ambiguous. However, the similarity between the preferred bunch structures and the shell structures of the corresponding Wigner molecules is already well established. For nine, ten, and eleven classical electrons confined in a 2D harmonic potential, the lowest-energy configurations

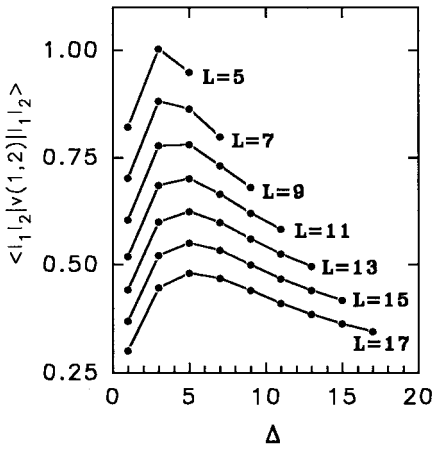

Figure 6. The interaction energies of two electrons in an unperturbed antisymmetric state $|l_1, l_2\rangle$, $\langle l_1, l_2|v(1,2)|l_1, l_2\rangle$, are presented as functions of $\Delta = |l_2 - l_1|$ for different values of $L_{12} = l_1 + l_2$. $\Delta = 1$ is the smallest value allowed by the Pauli principle. The energy unit is $e^2/(4\pi\epsilon_0\epsilon_r a)$.

are the two-shell structures (2, 7), (2, 8), and (3, 8) respectively [23–25]. This gives us a clue as regards why the bunch structure {2, 7} is preferred by the nine-electron quantum dot and {2, 8} is preferred by the ten-electron quantum dot when L is sufficiently large. For eleven classical electrons, the difference in energy between the global-minimum (3, 8) and the local-minimum (2, 9) configurations is only 0.06%. This explains why the bunch structures {2, 9} and {3, 8} are almost equally effective in reducing the Coulomb energy for eleven electrons in a quantum dot.

3.5. Effects of impurity

Up till now, our discussions have been limited to impurity-free dots. The implantation of an impurity ion can significantly change the spectrum of a quantum dot. If the impurity ion locates at the centre of the dot, L continues to be a good quantum number. In figure 7(a), η_0 is presented for a nine-electron dot with a negatively charged acceptor ion at the centre. Due to the repulsive electron–impurity interaction, any configuration having a few particles close to the centre is energetically quite unfavourable. As a result, the electrons tend to be in a single compact bunch, and a downward cusp in η_0 occurs when a compact filling is accessible (i.e., $L = 36, 45, 54, 63, \ldots$ for $N = 9$).

If the impurity is a positively charged donor ion, the attractive electron–impurity interaction favours a larger number n of particles close to the centre. With $N = 9$, the major η_0-cusps, occurring at states $|\{2, 7\}_k; L\rangle$ in an impurity-free dot, are shifted to states $|\{3, 6\}_k; L\rangle$ in a donor-doped dot in figure 7(b).

3.6. Summary

To summarize, in this paper we have presented a comprehensive analysis of the low-lying spectrum of electrons in the lowest Landau level in a quantum dot. Mixings of higher Landau levels are included through the high-order perturbation theory. Unlike systems with few electrons ($N < 7$), several-electron systems may have more than one sequence of magic numbers, which cannot be explained by the previous geometrical configuration model. The

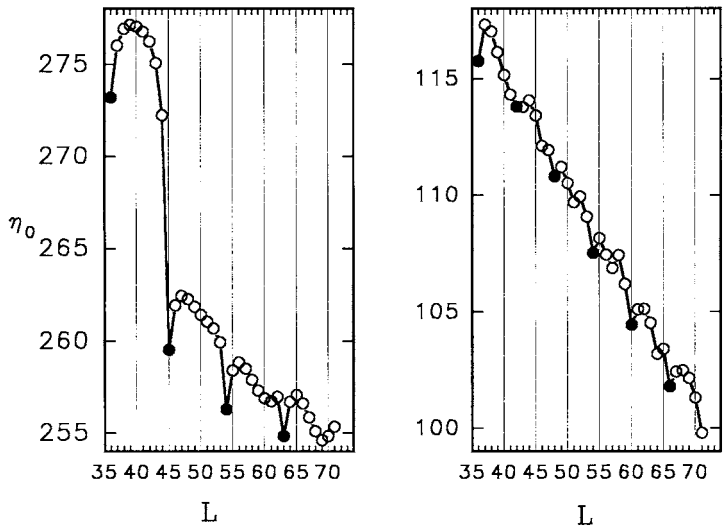

Figure 7. η_0 as a function of L for nine electrons in a quantum dot: (a) for an acceptor-doped quantum dot; (b) for a donor-doped quantum dot.

short-range attraction and long-range repulsion between two orbiting electrons favours certain bunch structures depending on N. Due to the quantization of angular momentum, the energetically favourable bunch structures are accessible only when L takes the magic values. We have carried out the calculations for $N = 12$, 13, and 14 and found that the preferred configuration is also a two-bunch structure. The three-bunch structure is expected to exist in systems with $N \geqslant 16$ and the four-bunch structure is expected to exist in systems with $N \geqslant 21$. Unfortunately they are beyond the scope of our numerical computations.

Acknowledgments

This work was supported by the Croucher Foundation, and also supported in part by the National Natural Science Foundation, grant No 19875018, Guangdong Natural Science Foundation and Guangzhou Natural Science Foundation, People's Republic of China.

References

[1] Ashoori R C 1996 *Nature* **379** 413
[2] McEuen P L, Foxman E B, Meirav U, Kastner M A, Meir Y and Wingreen N S 1991 *Phys. Rev. Lett.* **66** 1926
[3] Ashoori R C, Stormer H L, Weiner J S, Pfeiffer L N, Baldwin K W and West K W 1993 *Phys. Rev. Lett.* **71** 613
[4] Yang S-R E, MacDonald A H and Johnson M D 1993 *Phys. Rev. Lett.* **71** 3194
[5] Ahn K H, Oh J H and Chang K J 1995 *Phys. Rev.* B **52** 13 757
[6] Laughlin R B 1983 *Phys. Rev.* B **27** 3383
[7] Girvin S M and Jach T 1984 *Phys. Rev.* B **29** 5617
[8] Lai W, Yu K, Su Z and Yu L 1984 *Solid State Commun.* **52** 339
[9] Maksym P A and Chakraborty T 1991 *Phys. Rev. Lett.* **65** 108
Maksym P A and Chakraborty T 1992 *Phys. Rev.* B **45** 1947
[10] Maksym P A 1993 *Physica* B **184** 385
Maksym P A 1996 *Phys. Rev.* B **53** 10 871
[11] Hawrylak P and Pfannkuche D 1993 *Phys. Rev. Lett.* **70** 485
[12] Ruan W Y, Liu Y Y, Bao C G and Zhang Z Q 1995 *Phys. Rev.* B **51** 7942

[13] Bao C G, Ruan W Y and Liu Y Y 1996 *Phys. Rev.* B **53** 10 820
[14] Seki T, Kuramoto Y and Nishino T 1996 *J. Phys. Soc. Japan* **65** 3945
[15] Ruan W Y and Cheung Ho-Fai 1999 *J. Phys.: Condens. Matter* **11** 435
[16] Jain J K and Kawamura T 1996 *Europhys. Lett.* **29** 321
[17] Kawamura T and Jain J K 1996 *J. Phys.: Condens. Matter* **8** 2095
[18] Dharma-wardana M W C 1995 *J. Phys.: Condens. Matter* **7** 4095
[19] Delves L M 1959 *Nucl. Phys.* **9** 391
Lin C D 1995 *Phys. Rep.* **257** 2
[20] Taut M 1993 *Phys. Rev.* A **48** 3561
[21] Merkt U, Huser J and Wagner M 1991 *Phys. Rev.* B **43** 7320
[22] Chamon W and Wen X G 1994 *Phys. Rev.* B **49** 8227
[23] Bedanov V M and Peeters F M 1994 *Phys. Rev.* B **49** 2667
[24] Choi M F, Cheung P and Hui P M 1997 *Solid State Commun.* **103** 357
[25] Xie W F and Chen C Y 1998 *Physica* B **254** 207